Journal of Neuroimmunology 222 (2010) 48–61

Contents lists available at ScienceDirect

Journal of Neuroimmunology

journal homepage: www.elsevier.com/locate/jneuroim

Intracerebroventricular Shiga toxin 2 increases the expression of its receptor globotriaosylceramide and causes dendritic abnormalities

Carla Tironi-Farinati [a], C. Fabián Loidl [b], Javier Boccoli [a], Yanil Parma [c], Mariano E. Fernandez-Miyakawa [c], Jorge Goldstein [a,*]

[a] Laboratorio de Neurofisiopatología, Departamento de Fisiología, Facultad de Medicina, Universidad de Buenos Aires, Paraguay 2155 piso 7, CABA (1121), Argentina
[b] Instituto de Biología Celular y Neurociencia "Prof. E. De Robertis," Facultad de Medicina, Universidad de Buenos Aires, Paraguay 2155 piso 3, CABA (1121), Argentina
[c] Instituto de Patobiología, Centro Nacional de Investigaciones Agropecuarias, Instituto Nacional de Tecnología Agropecuaria, Calle Las Cabañas y Los Reseros s/n, Casilla de Correo 25 (1712), Castelar, Buenos Aires, Argentina

ARTICLE INFO

Article history:
Received 2 October 2009
Received in revised form 26 February 2010
Accepted 2 March 2010

Keywords:
Gb_3
Shiga toxin 2
Neuronal damage
MAP2
GFAP
Intracerebroventricular

ABSTRACT

Neurological damage caused by intoxication with Shiga toxin (Stx) from enterohemorrhagic *Escherichia coli* is the most unrepairable and untreatable outcome of Hemolytic Uremic Syndrome, and occurs in 30% of affected infants. In this work intracerebroventricular administration of Stx2 in rat brains significantly increased the expression of its receptor globotriaosylceramide (Gb_3) in neuronal populations from striatum, hippocampus and cortex. Stx2 was immunodetected in neurons that expressed Gb_3 after intracerebroventricular administration of the toxin. Confocal immunofluorescence of microtubule-associated protein 2 showed aberrant dendrites in neurons expressing increased Gb_3. The pro-apoptotic Bax protein was concomitantly immunodetected in neurons and other cell populations from the same described areas including the hypothalamus. Confocal immunofluorescence showed that Gb_3 colocalized also with glial fibrillary acidic protein only in reactive astrocytic processes, and not in vehicle-treated normal ones. Rats showed weight variation and motor deficits as compared to controls. We thus suggest that Stx2 induces the expression of Gb_3 in neurons and triggers neuronal dysfunctions.

1. Introduction

Infection by Shiga toxin (Stx)-producing enterohemorrhagic *Escherichia coli* (STEC) causes hemorrhagic colitis and Hemolytic Uremic Syndrome (HUS) (O'Brien and Kaper, 1998), characterized by thrombocytopenia, microangiopathic hemolytic anemia and acute renal failure (Proulx et al., 2001; Karmali, 2004).

Central nervous system (CNS) complications are observed in around 30% of the infant population with HUS. Patients may be affected with acute seizures, coma, irritability, hemiparesis or motor disorders (Eriksson et al., 2001; Valles et al., 2005).

Stx2 is a protein composed of a 32-kDa subunit A (StxA) and five 7.7-kDa subunits B (StxB). StxA bears N-glycosidase activity, depurinates the rRNA 28S, inhibits protein biosynthesis and promotes host cell death (Lord et al., 2005). Therefore StxA must be transported to the cytosol by StxB (Johannes and Decaudin, 2005; Sandvig and van Deurs, 2005). StxB binds with high affinity to the cell membrane of the globotriaosylceramide (Gb_3) cell membrane Gb_3 receptor, allowing Stx to be internalized into endosomes towards the trans-Golgi network (Mallard et al., 1998).

Gb_3 is synthesized from lactosylceramide by α1,4-galactosyltransferase (Okuda and Nakayama, 2008). Binding of StxB to Gb_3 induces intracellular signals dependent on glycolipid-enriched membrane domains (Falguières et al., 2001; Takenouchi et al., 2004). Consequently, Stx may cause apoptosis in cells expressing Gb_3 in human brain endothelial cells (Fujii et al., 2008) and combined with either LPS (Louise and Obrig, 1992) or cytokines (Louise and Obrig, 1991) in HeLa cells (Fujii et al., 2003) or in the renal epithelium (Psotka et al., 2009). Also, TNF-α upregulates Gb_3 and confers sensitivity to different types of endothelial cells (Eisenhauer et al., 2001; Louise and Obrig, 1991).

Gb_3 cell localization and expression may vary in different cell populations in the nervous systems of different animal species, either treated or not with Stx2. It has been reported that normal rat and mouse dorsal root ganglion neurons express Gb_3 (Ren et al., 1999). Normal mouse central nervous system neurons have also been reported to express Gb_3 (Obata et al., 2008). In addition, the expression of Gb_3 in peripheral and central nervous system seems to have a correlation in humans, as it is expressed in vessels and neurons of the nervous system (Ren et al., 1999; Obata et al., 2008). For instance, it has been reported that Stx2 increases neuronal transmitter release in murine brain slices (Obata et al., 2008). Also, changes in the expression of the neurotransmitter nitric oxide and

Abbreviations: Gb_3, Globotriaosylceramide; MAP2, Microtubule-associated protein 2; GFAP, Glial fibrillary acidic protein; Stx2, Shiga toxin 2.

* Corresponding author. Tel.: +54 11 5 950 9500x2141; fax: +54 11 4 964 0503.
E-mail address: jogol@fmed.uba.ar (J. Goldstein).

0165-5728/$ – see front matter © 2010 Elsevier B.V. All rights reserved.
doi:10.1016/j.jneuroim.2010.03.001

reactive astrocytes have also been observed in rat brains (Boccoli et al., 2008). In rabbit brains, Stx2 might damage neuronal cells by the inflammatory response that occurs in endothelial cells expressing Gb_3 (Takahashi et al., 2008). In addition, expression of Gb_3 has been found in neurons and endothelial cells of normal motor cortex from brains of human cadavers (Obata et al., 2008).

As an attempt to determine whether Stx2 could affect rat brains by possessing a direct neurotoxic involvement, in the present work we studied the role of Stx2 in brain injury. Our group has previously investigated the effects of the i.c.v. administration of Stx2 at the ultrastructural level (Goldstein et al., 2007). This approach discarded the synergistic effect of Stx2 with the pro-inflammatory cytokines TNF-α and IL-1β produced in circulatory endothelial cells (Paton and Paton, 1998). Accordingly, (in that work) we observed the highest incidence of brain damage after 8 days of i.c.v. administration of Stx2. This event included neuronal apoptosis, hypertrophic and demyelinated axons, the immunoelectron localization of Stx2 in these axons and in the nuclei of astrocytes, astrocytic cytoplasmic edema and gliosis, and demyelinated sheaths in oligodendrocytes. It has been postulated that Stx2B may be involved in the inhibition of rRNA assembly occurring in the nucleus (Falguieres and Johannes, 2006). Since neuronal apoptosis may be caused by the action of endocytosed Stx2, rat brain neurons may express a Gb_3 receptor for the toxin.

In the present work we seek to obtain new knowledge for the role of the Stx2 receptor Gb_3, in an attempt to further address the neurological damage caused by Stx2 from enterohemorrhagic *E. coli*.

Stx2 may produce changes in the expression of its Gb_3 receptor in neurons, and concomitantly alter the expression of the proteins involved in neuronal plasticity and synapsis. Apoptotic neurons found at the ultrastructural level (Goldstein et al., 2007) may express pro-apoptotic proteins. These events may occur in a reactive astrocytic scenario, a characteristic of the area of brain damage.

To address these issues, the aims of the present study were: (i) to assess whether Stx2 can induce changes in the expression of the Gb_3 receptor in the rat brain, (ii) to investigate the effects of Stx2 on the expression of the cytoskeletal protein MAP2 related to dendritic structure and synaptic plasticity (for review refer to Sánchez et al., 2000), (iii) to determine whether Gb_3 induction by Stx2 occurs in a reactive astrocytic area, and (iv) to correlate these events as a result of the expression of the pro-apoptotic Bax protein in neurons.

2. Materials and methods

2.1. Stx2 protein purification

Stx2 was purified by affinity chromatography under native conditions. The Stx2 purification procedures have been previously described and characterized (Goldstein et al., 2007). Briefly, recombinant *E. coli* DH5α containing pStx2 were cultured overnight in LB supplemented with 100 μg/ml ampicillin. The culture was centrifuged and the supernatant was precipitated in 60% $SO_4(NH_4)_2$ 1 mM PMSF following precipitation at 12,000 rpm at 4 °C for 20 min. The concentrate was dialized to remove the $SO_4(NH_4)_2$ overnight with 4 volumes of PBS. The pellet obtained was resuspended in PBS with a cocktail of protease inhibitors (20 mM leupeptin, 1 mM aprotinin, 10 uM pepstatin A, 1 mM PMSF) and incubated with the Globotriose Fractogel Resin (IsoSep AB, Tullinge, Sweden) for 4 h at 4 °C. The resin was washed and eluted with $MgCl_2$. The protein concentration in all the eluates was followed measuring the absorption at 280 nm, and the toxin was aliquoted and stored at −70 °C. Protein content of all the fractions was monitored by Silver Coomassie Blue (Candiano et al., 2004), and the presence of Stx2 was confirmed by Western Blot, which showed a 7.7-kDa band corresponding to Stx2B and a 32-kDa band corresponding to Stx2A. The cytotoxic capacity of Stx2 was assessed in Vero cells by neutral red assay for 72 h and the cytotoxic dose 50 (CD_{50}) found was about 1 pg/ml (Fig. 1A). This effect was

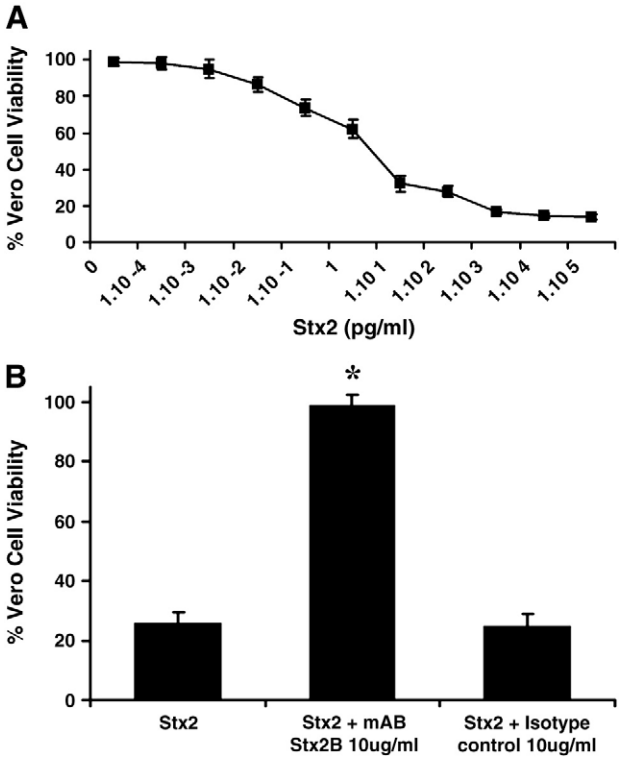

Fig. 1. Stx2 obtained by affinity chromatography purification was cytotoxic to Vero cells. The Stx2 cytotoxic capacity was confirmed on a Vero monolayer cell culture (A). Preincubation of the toxin with a monoclonal anti-Stx2B antibody resulted in a significant increase in Vero cell viability, while that with an isotype monoclonal antibody had no neutralizing effect (B). Data are reported as means ± S.E.M. of at least three triplicate experiments (*$p<0.05$).

neutralized by means of preincubation with an anti-subunit 2B monoclonal antibody (Sifin, Berlin, Germany), and not neutralized when using an isotype antibody instead (Fig. 1B).

Another set of control experiments was performed to demonstrate that an i.c.v. administration of 50 ng/ml of lipopolysaccharide (LPS) alone (without Stx2) does not increase the (levels of) the Gb_3 receptor. Consequently, LPS was removed from the Stx2 solution to use it for additional experiments aimed to demonstrate that Gb_3 neuronal expression was increased only by the i.c.v. of Stx2. LPS was removed from the Stx2 solution by using Detoxi-gel (Pierce, Rockford, USA). This Stx2 solution contained less than 0.03 EU/ml.

2.2. Vero cell culture

Vero cells were maintained in DMEM supplemented with 10% fetal calf serum. Cells were seeded in 96-well plastic microplates for cytotoxicity assays to 90% confluency. Cytotoxicity experiments were carried out without serum.

2.3. Animals

Male Sprague–Dawley rats (250–300 g) were housed in an air-conditioned and light-controlled (lights between 06:00 and 18:00 h) animal facility. Rats were provided with food and water *ad libitum*. They were daily monitored for weight and observed for neurological manifestations from the beginning of the experiment until the last day, always at the same time. After 8 days of i.c.v. Stx2, Stx2 free of LPS, LPS (Sigma, St. Louis, MO, USA) or vehicle infusions, the rats were killed for confocal immunofluorescence studies. Rats were anesthetized with Chloral hydrate (350 mg/kg) and perfused transcardially with 0.9% NaCl solution followed by 4% paraformaldehyde in 0.1 M phosphate buffer solution (PBS) [fixative per animal weight (ml/g)]. Brains were removed from the skull, and post-fixed in the same fixative solution for 2 h. Brain

sections were cut on an Oxford vibratome. Serial 40-μm-thick coronal sections were obtained and collected in 0.1 M Phosphate Buffer. Brain floating sections obtained were subsequently processed for immunofluorescence.

The experimental protocols and euthanasia procedures were reviewed and approved by the Institutional Animal Care and Use Committee of Buenos Aires University, School of Medicine (Resolution N° 2079/07).

2.4. infusion of Stx2

Anesthetized male rats (ketamine 50 mg/kg–diazepam 0.35 mg/kg, i.p.) were stereotaxically implanted into the lateral ventricle with a stainless steel guide cannula (Plastic One, Roanoke, VA). The placement coordinates were anteroposterior: −1.80 mm; lateral: 2.4 mm and vertical: 3.2 mm (Paxinos and Watson, 2005). To reach the ventricle area and minimize the damage of tissue, a 21-gauge guide cannula was implanted at this point. Then, a 30-gauge needle extending 0.5 mm below the guide cannula was used for the injections. The correct placement of the ventricle cannulae was verified at the end of the experiment, followed by postmortem brain fixation and cut on an Oxford vibratome; data obtained from improperly implanted animals were excluded from the analyses. Cannulae were fixed to the skull surface with three screws and dental acrylic cement and temporarily occluded with dummy cannulae. After surgery, animals were caged individually. Rats were randomly assigned to different experimental groups and each rat was used only once. One week after the surgery, freely moving animals were i.c.v. injected through a 30-gauge needle connected by polyethylene tubing to a 20-μl Hamilton syringe. The needle was left in place for 30 s to prevent backflow of the injected solution. The rats were i.c.v. injected with either vehicle or 12 and 24 pg of Stx2 per gram of animal weight. After 2, 4 and 8 days, the rats were killed for confocal immunofluorescence studies.

2.5. Immunofluorescences of Stx2, Gb_3, MAP2, GFAP and Bax

2.5.1. Visualization of Gb_3 and Stx2

Brain floating sections were incubated with normal goat serum 1% (Sigma, St. Louis, MO, USA) for 1 h in PBS, following incubation with monoclonal anti-Stx2B antibody, dilution 1:100 (Sifin, Berlin, Germany) at 4 °C for 72 h in PBS and after several rinses with the same buffer, the sections were subsequently incubated with goat IgG anti-mouse/Texas Red, dilution 1:200 (Sigma, St. Louis, MO, USA) for 1 h in PBS, copiously rinsed in PBS again, and incubated with Hoescht 33342 (blue) 1 μg/ml (Sigma, St. Louis, MO, USA) for 30 min in PBS. Then the same sections were incubated with Rat IgM anti-CD77/Gb_3 antibody, dilution 1:100 (Beckman Coulter, Brea, California, USA) for 48 h at 4 °C in PBS and after several rinses with the same buffer incubated with Anti-rat IgMb FITC (green), dilution 1:400 for 1 h (Jackson, PA, USA). The same procedure was used for confocal immunofluorescence on brain sections for Gb_3 localization in Figs. 3 and 4. Micrographs were obtained with a Zeiss Axiophot microscope.

2.5.2. Visualization of Gb_3 and MAP2

Brain floating sections were incubated with normal goat serum 1% (Sigma, St. Louis, MO, USA) for 1 h in PBS, following incubation with mouse monoclonal anti-MAP2 antibody, dilution 1:500 (Sigma, St. Louis, MO, USA) at 4 °C for 72 h in the same buffer, and after several rinses with PBS the sections were subsequently incubated with goat IgG anti-mouse/Texas Red, dilution 1:200 (Sigma, St. Louis, MO, USA), copiously rinsed in PBS again. After that, Gb_3 immunofluorescence was performed in the same brain sections as described above.

2.5.3. Visualization of Gb_3 and GFAP

Brain floating sections were incubated with BSA 1% (Sigma, St. Louis, MO, USA) for 1 h in 10 mM PBS, following incubation with polyclonal rabbit antibody against GFAP, dilution 1:500 (Sigma, St. Louis, MO, USA) at 4 °C for 48 h diluted in 10 mM PBS + 0.2% Triton X-100. After that, a secondary goat IgG anti-rabbit Cy3, dilution 1:100 (Zymed Laboratories Inc, San Francisco, CA, USA) was incubated for 1 h in 10 mM PBS. Gb_3 immunofluorescence was then performed in the same brain sections as described above.

2.5.4. Visualization of Bax

Brain floating sections were incubated with goat normal serum 2% (Sigma, St. Louis, MO, USA), following incubation with mouse monoclonal anti-Bax antibody, dilution 1:500 (Santa Cruz Biotechnology, Santa Cruz, CA, USA) in 10 mM PBS + 0.2% Triton X-100 at 4 °C for 48 h. After several rinses in the same buffer a secondary biotinylated goat IgG anti-mouse, dilution 1:200 (Invitrogen Molecular Probes, Carlsbad, California, USA) in 10 mM PBS was incubated for 1 h, and following several washes with the same buffer the sections were incubated with Streptavidin Alexa Fluor 488 (Invitrogen Molecular Probes, Carlsbad, California, USA) for 1 h in 10 mM PBS.

2.5.5. Controls

Negative controls were carried out using the same procedure but omitting the primary antibody. Isotype controls were used in each case: mouse monoclonal anti-BrdU (Sigma, St. Louis, MO, USA), mouse IgG (Sigma, St. Louis, MO, USA) (controls for Stx2 and MAP-2 respectively), rat IgM antibody (1:50) (F104UN, American Qualex, San Clemente California) (for Gb3 isotype control).

2.6. Confocal imaging

Confocal colocalization images were carried out by gray-scale images (12 bit), acquired with an Olympus FV300 confocal microscope using the green helium–neon laser (543 nm) and argon laser (488 nm). Images were captured with Fluo View application software. Serial optical sections were performed with Simple 32 C-imaging computer. Z series sections were collected at 1 μm with an Uplan Apo 20× or 40×. Images were taken with a scan zoom of ×1. Adobe Photoshop and Image J (NIH) software was used to assemble the images and obtain merged images. Stx2 and Gb3 colocalization photos were taken with a Zeiss Axiophot microscope.

2.7. Integral optical density (IOD) frequency analysis of Gb_3, MAP2 and GFAP expression levels

Gb_3, MAP2 and GFAP-immunopositive cells were visualized using ×10 and ×40 objective lenses. All analyses were carried out in

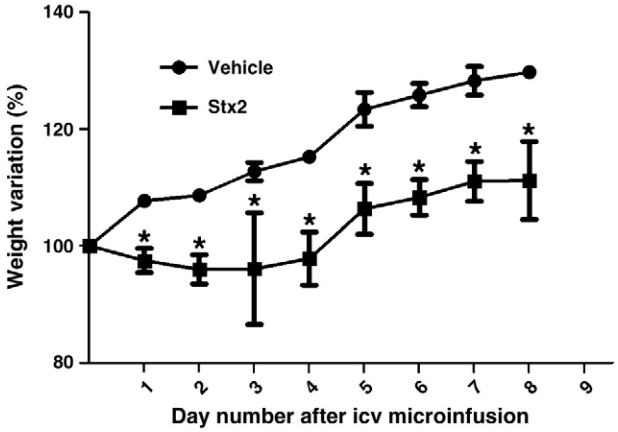

Fig. 2. Weight variation after Stx2 i.c.v. administration. Weight was monitored for 8 days after the Stx2 or vehicle local microinfusion; significant differences between treatments were found after the first day of treatment (*$p<0.05$).

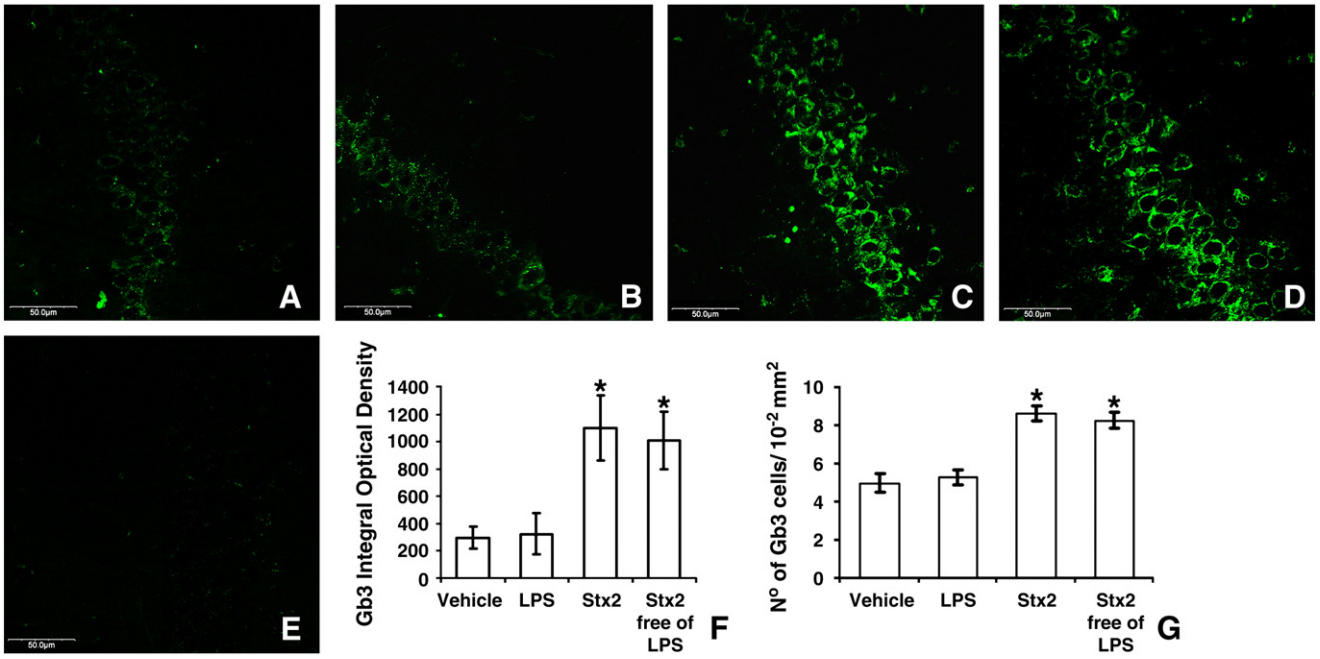

Fig. 3. The area observed in this study is located in the rat CA1 hippocampus (Fig. 5J). Confocal immunofluorescence micrographs show that the i.c.v. injection of 24 pg/g of Stx2 per gram of animal weight or of 24 pg/g of Stx2 free of LPS increased the expression of Gb_3 in the hippocampus (C and D respectively) and that Gb_3 expression was diminished after i.c.v. injection of 50 ng/ml of LPS or vehicle (B and A respectively). Integral optical density (IOD) measurements (F) confirmed that Gb_3 expression level was higher in the brains treated with Stx2 or Stx2 free of LPS, as compared with those treated with LPS alone or vehicle. No significant differences in the levels of Gb_3 expression were found after the injection of Stx2 and those after the injection of Stx2 free of LPS (F). The number of Gb_3 immunopositive cells was higher in the brains treated with Stx2 or Stx2 free of LPS, as compared with those treated with LPS alone or vehicle (G). An isotype control is shown (E). $^*p<0.05$.

comparable areas under the same optical and light conditions. Confocal images were taken with the same confocal settings on an Olympus FV300 microscope. The immunofluorescence integrated intensities inside each cell body perimeter were measured using ImageJ (NIH), the background integrated density was also calculated to obtain the corrected integrated density (cell total integrated density–background integrated density) for each photograph. Hoechst nuclear staining was performed to count the number of positive cells and MAP2 immunofluorescence was used to count dendrites by using the ImageJ Cell counter plugin. Cells and dendrites that were above the threshold level were counted as positive for that marker.

2.8. Statistical analysis

Five brain sections from each of six animals, i.e., a total of 30 for each condition for i.c.v. Stx2 microinfusion, and the same number for

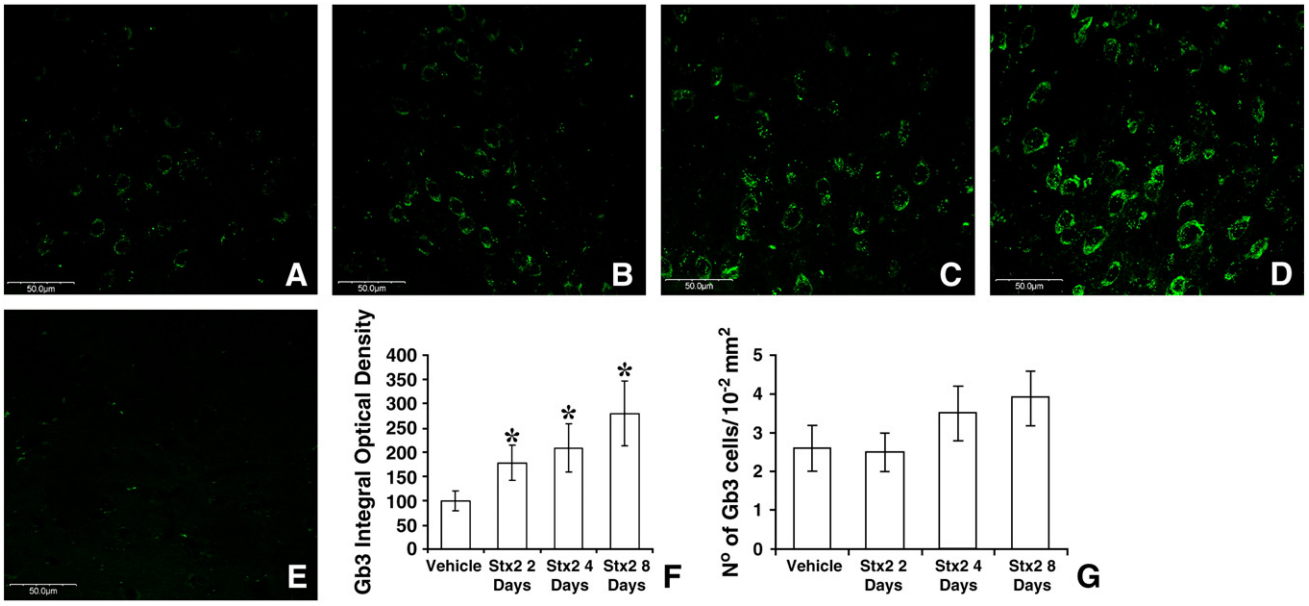

Fig. 4. The area observed in this study is located in the rat corpus striatum (Fig. 7J). Time course of Gb_3 expression following i.c.v. injection of Stx2 (A–D). A confocal immunofluorescence micrograph shows a control obtained from vehicle i.c.v. administration (A). After 2, 4 and 8 days of Stx2 i.c.v. administration (B–D) increasing Gb_3 expression can be observed along the time. An isotype control is shown (E). IOD measurements (F) confirmed that Gb_3 expression level increased until day 8 after toxin administration. No significant difference was found in the number of neurons expressing this receptor (G). $^*p<0.05$.

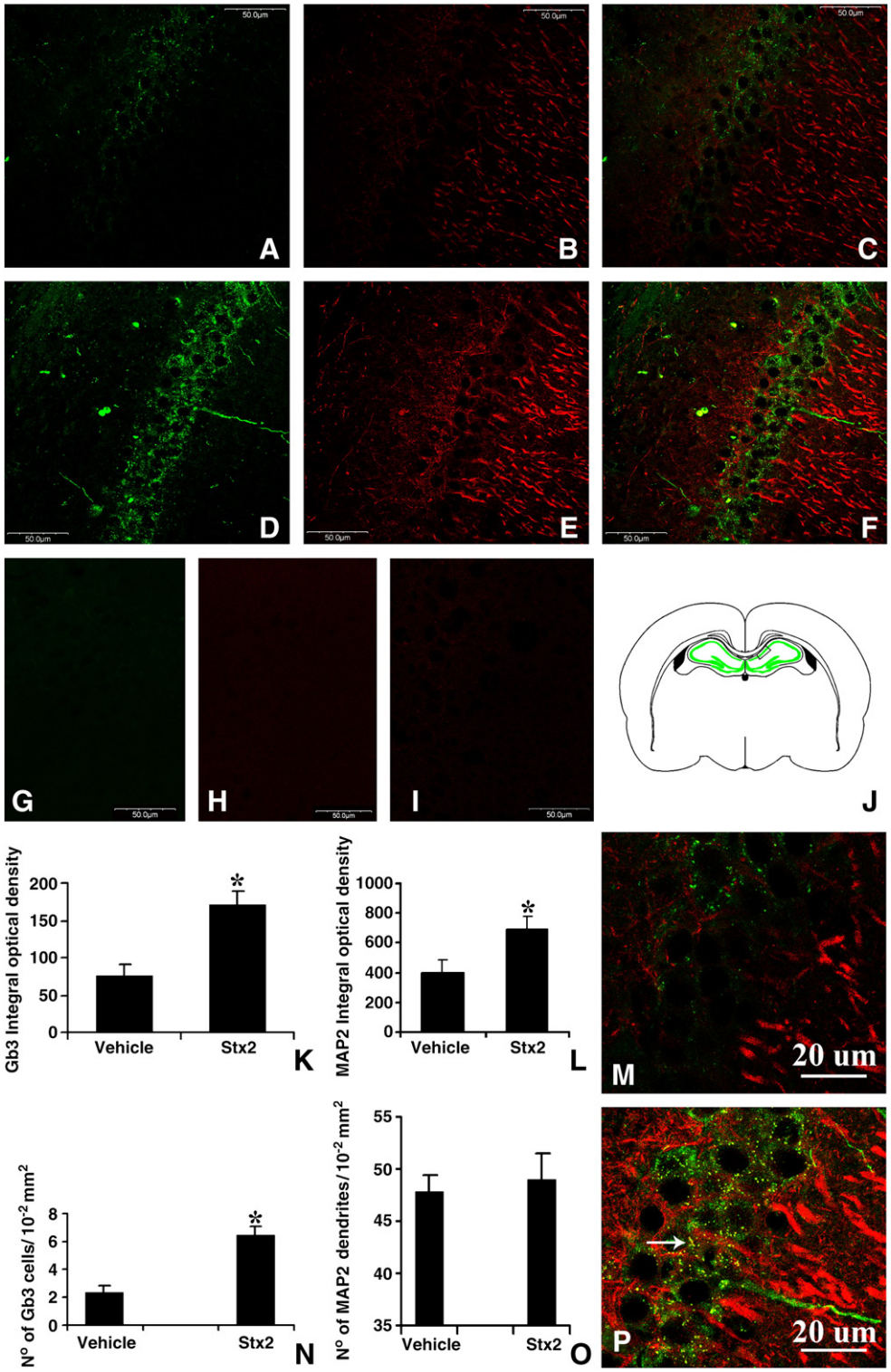

Fig. 5. The local administration of Stx2 increased the expression of the receptor Gb_3 in the rat CA1 hippocampus. Confocal immunofluorescence micrographs for Gb_3 and MAP2 are shown in green (A and D) and red (B and E) respectively, and merging images are observed in C and F. Representative vehicle- (A–C) and Stx2-treated (D–F) animals are shown. Stx2 increased the expression of Gb_3 (D) in neurons, together with an increased expression of MAP2 (E), as compared with the vehicle-treated animals (A and B, respectively). Isotype control micrographs for Gb_3 and MAP2 (G and H) showed no immunoreaction. A negative control for MAP2 is shown (I). The area observed in this study is located inside the rectangle in J. All these data were confirmed by IOD analysis in which Stx2 induced the expression of Gb_3 (K) and a higher number of positive Gb_3 cells per field were found (N). Cells were identified by using Hoechst nuclear staining (representative micrographs of nuclear fluorescent staining can be visualized on Fig. 11). IOD analysis also showed that MAP2 increased after Stx2 i.c.v. administration (L), although the number of MAP2 positive dendrites did not show any changes (O). A higher magnification of micrographs from vehicle- (M) and Stx2-treated (P) animals is shown. Colocalization between Gb_3 and MAP2 immunofluorescence in yellow can be observed in a granule-shaped pattern (arrow, P). This is not observed in the vehicle-treated rats (M). Statistical significance is shown with an asterisk, $^{*}p<0.05$.

the vehicle condition, were used for confocal IOD analysis and then statistically analyzed by quantitative immunofluorescence studies. Results are expressed as the mean ± SE. Student's *t* test, one-way ANOVA followed by the Student–Newman–Keuls multiple comparison test, or two-way repeated measures ANOVA followed by multiple comparison were used. The criterion for significance was $p<0.05$.

3. Results

3.1. Weight variation and neurological manifestations after i.c.v administration of Stx2

We have previously determined that the highest incidence of brain damage occurs after 8 days of i.c.v. administration of Stx2 (Goldstein et al., 2007). Weight variation was determined for both groups (toxin- and vehicle-treated). A trend of weight gain compared to their initial weight was observed for both groups (Fig. 2). On the other hand, rats lost weight after i.c.v administration of Stx2 as compared to the vehicle at every time point given. This was continuously monitored starting from day 1 of intoxication until day 8 ($n=6$) (Fig. 2). A statistically significant weight loss was observed beginning from day 1 and throughout the experiment of toxin treatment as compared with the control. Rats died after 8 days of i.c.v. Stx2 treatment. Abnormal neurological manifestations started with hypokinesia on day 4, and followed by lethargy, subsequent hind-limb weakness, crawling and paralysis. On days 6 to 7, rats started with spontaneous seizures. In contrast, animals i.c.v microinjected with saline did not evidence weight loss and/or neurological abnormalities.

3.2. Increased Gb_3 expression in neurons is due to Stx2

In order to determine whether Stx2 is responsible for an increase in Gb_3 expression, rats were i.c.v. injected with either Stx2, Stx2 following removal of LPS (Stx2 free of LPS), only LPS, or vehicle (Fig. 3). We observed that after 8 days of the i.c.v. injection of LPS the expression of Gb_3 did not significantly differ from that after injection of vehicle in neurons of CA1 hippocampus (Fig. 3B, A). Moreover, the expression of Gb_3 was increased in hippocampal CA1 neurons after i.c.v. injection of Stx2 (Fig. 3C) in comparison with the treatments with either vehicle or LPS (Fig. 3A, B). No differences in neuronal Gb_3 expression in this brain area were detected between i.c.v. injections of Stx2 and Stx2 free of LPS (Fig. 3C, D) as revealed by confocal immunofluorescence microscopy. These data were confirmed by integral optical density (IOD) measurements on Gb_3 expression levels (Fig. 3F). In addition, the number of positive Gb_3 neurons was maximum ($p<0.05$) after the injection of Stx2 and/or of Stx2 free of LPS as compared to that after the injection of vehicle or LPS (Fig. 3G).

3.3. Local administration of Stx2 increases the expression of Gb_3, until day 8

To test whether i.c.v. injection of Stx2 increases the expression of the receptor Gb3 in a time course manner, toxin- or vehicle-treated striata from rat brains were analyzed by confocal immunofluorescence (Fig. 4). We found that the expression of Gb_3 was significantly higher than controls starting from day 2 and until day 8 (Fig. 4A–D). All the preceding data were measured by integral optical density (IOD) (Fig. 4F). No significant difference was found in the number of neurons expressing this receptor along the observed days (Fig. 4G).

3.4. Local administration of Stx2 increases the expression of the receptor Gb_3 and altered MAP2 expression in different neuronal rat brain populations

Double immunofluorescence confocal microscopy was used to assay the immunodistributions of the receptor Gb_3 and MAP2, a cytoskeleton neuronal marker abundantly found in neuronal bodies and postsynaptic dendrites.

CA1 hippocampal neurons (Fig. 5J) immunoexpressing MAP2 contained the Gb_3 receptor immunolabeled in a granular shape (Fig. 5C, F, M, P). This was evidenced in the hippocampus treated with the toxin (Fig. 5P), compared to the vehicle (Fig. 5M). Gb_3 basal expression was immunolocalized in neurons of the hippocampal CA1 layer (Fig. 5A). After i.c.v. administration of the toxin, the expression of the Gb_3 receptor was found increased in comparison to the animals with vehicle administration (Fig. 5D, A). These data were supported by optical density analysis (Fig. 5K, $p<0.05$). Moreover, the number of positive neurons immunoexpressing Gb_3 was higher than that from the vehicle-treated rats (Fig. 5N, $p<0.05$). MAP2 immunoexpression in neurons of hippocampal CA1 layer from the vehicle-treated rats was evidently confined to neuronal fibers (Fig. 5B), while that in the toxin-treated hippocampuses was not only observed in neuronal fibers, but was also found increased in their cytoplasms (Fig. 5E). While there were no significant difference ($p<0.05$) between the number of dendrites immunoexpressing MAP2 in vehicle- and toxin-treated hippocampuses (Fig. 5O), optical density analysis showed that the hippocampuses treated with the toxin immunoexpressed MAP2 more than the vehicle-treated ones (Fig. 5L) ($p<0.05$). Isotype controls for Gb_3 and MAP2 immunoexpressions (Fig. 5G and H respectively) and a negative MAP2 control (Fig. 5I) validated these data.

In addition, MAP2 immunopositive dendrites of CA1 hippocampus treated with i.c.v. injection of Stx2 were found to be wider than the ones treated with the vehicle (Fig. 6).

Merging images expressing MAP2 and the Gb_3 receptor were also immunolocalized in neurons of vehicle- and toxin-treated striata (Fig. 7C, F, J, L, O). The Gb_3 receptor was also found in a granular shape in neurons from vehicle-injected striata, and immunoexpression of this receptor increased after toxin treatment (Fig. 7A, D). These data were supported by optical density analysis (Fig. 7K, $p<0.05$). However, no significant difference was found in the number of neurons expressing this receptor between both treatments (Fig. 7N, $p<0.05$). While there were no significant differences in the number of dendrites expressing MAP2 between both treatments (Fig. 7O, $p<0.05$), MAP2 optical density immunoexpression was found higher in striatal fibers and cytoplasms of neurons treated with Stx2 (Fig. 7L $p<0.05$), as observed in the confocal images (Fig. 7B, E). Isotype controls for Gb_3 and MAP2 immunoexpressions (Fig. 7G and H respectively) and a negative MAP2 control (Fig. 7I) validated these data.

Merging images of neurons expressing MAP2 and the Gb_3 receptor were observed by confocal microscopy of vehicle- or Stx2-treated cortexes (Fig. 8C, F, J, M, P).

Immunolocalization of the Gb_3 receptor was also found in vehicle-treated cortical neurons (Fig. 8A). Also, after Stx2 administration Gb_3 expression increased, predominantly in neurons from the inner cortex (Fig. 8D). These data were validated by optical density analysis

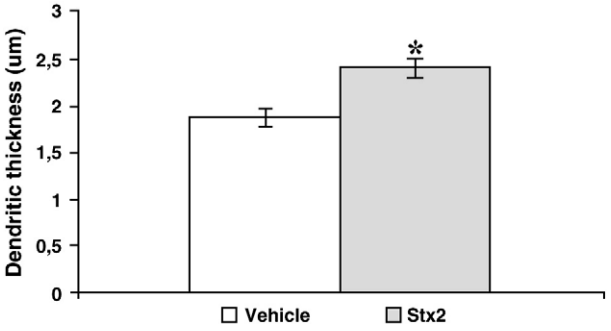

Fig. 6. A significant difference is shown between the thickness of dendrites from CA1 hippocampus treated with i.c.v. injection of Stx2 and that of those treated with the vehicle (*$p<0.05$).

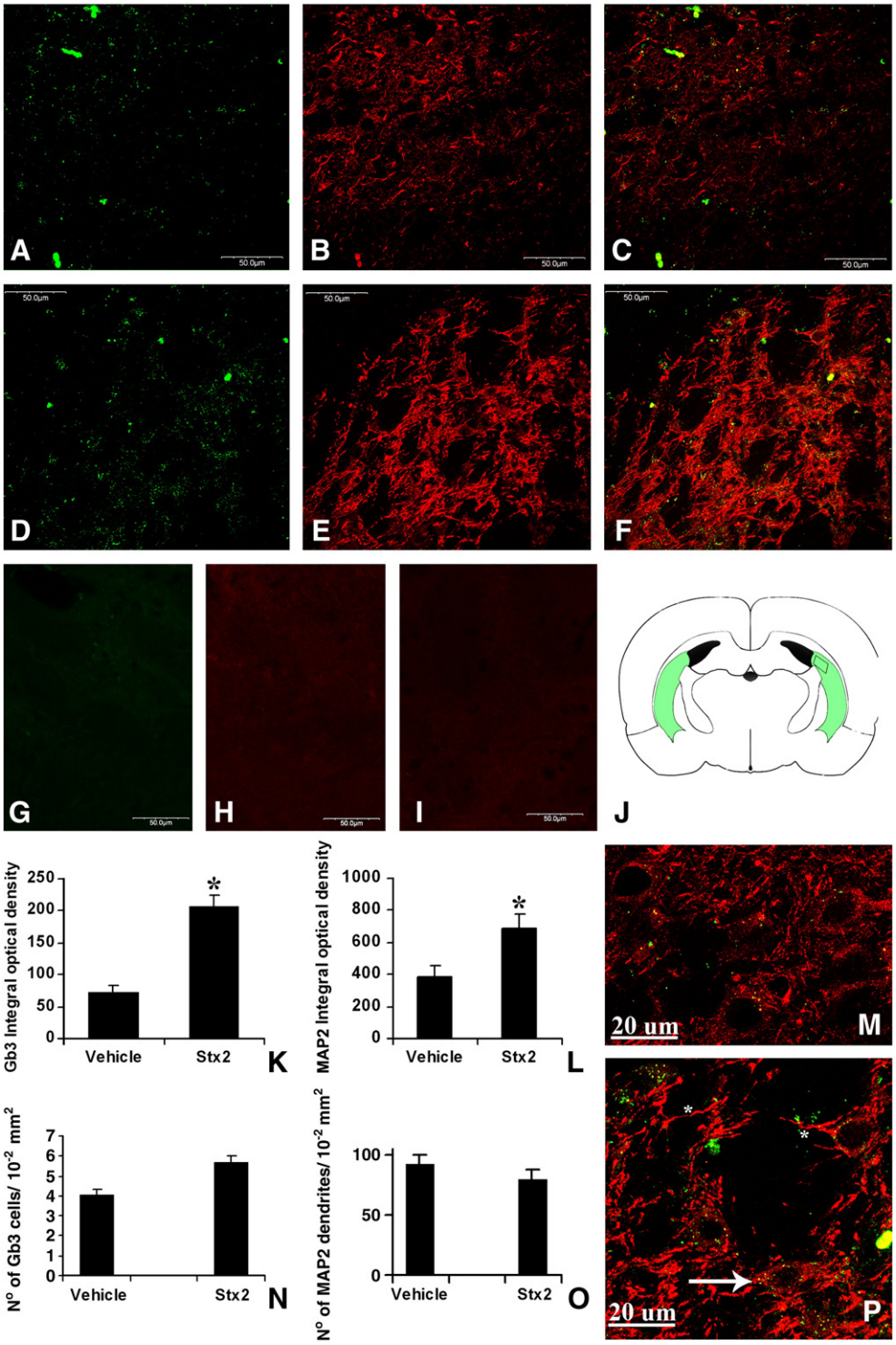

Fig. 7. The local administration of Stx2 increased the expression of the receptor Gb_3 in the rat dorsal striatum. Confocal immunofluorescence micrographs for Gb_3 and MAP2 are shown in green (A and D) and red (B and E) respectively, and merging images are observed in C and F. Representative vehicle- (A–C) and Stx2-treated (D–F) animals are shown. Stx2 increased the expression of Gb_3 (D) in neurons together with increased expression of MAP2, due to dendritic swelling (E) as compared with the vehicle-treated rats (A and B, respectively). Isotype controls micrographs for Gb_3 and MAP2 (G and H) showed no immunoreaction. A negative control for MAP2 is shown (I). The area observed in this study is marked in J. All these data were confirmed by IOD analysis in which Stx2 induced the expression of Gb_3 (K), while no significant differences were found in the number of positive Gb_3 cells per field between both groups (N). Cells were identified by using Hoechst nuclear staining (representative micrographs of nuclear fluorescent staining can be visualized in Fig. 11). IOD analysis also showed that MAP2 increased after Stx2 i.c.v. administration (L), although the number of MAP2 positive dendrites did not show any changes (O). A higher magnification of micrographs from vehicle- (M) and Stx2-treated (P) animals is shown. Colocalization between Gb_3 and MAP2 immunofluorescence in yellow can be observed in a granule-shaped pattern (arrow, P). This is less frequent in the vehicle (M). Statistical significance is shown with an asterisk, $p<0.05$. Focal dendritic swelling is shown (asterisk, P).

(Fig. 8K, $p<0.05$). However, no significant differences were found in the number of neurons in the same area analyzed for inner cortexes between vehicle- and Stx2-treated rats (Fig. 8N). In the inner cortex, however, MAP2 immunoexpression did not show differences between the vehicle- and Stx2-treated rats (Fig. 8L, O). Isotype and negative controls (Fig. 8G, H, I) validated these data.

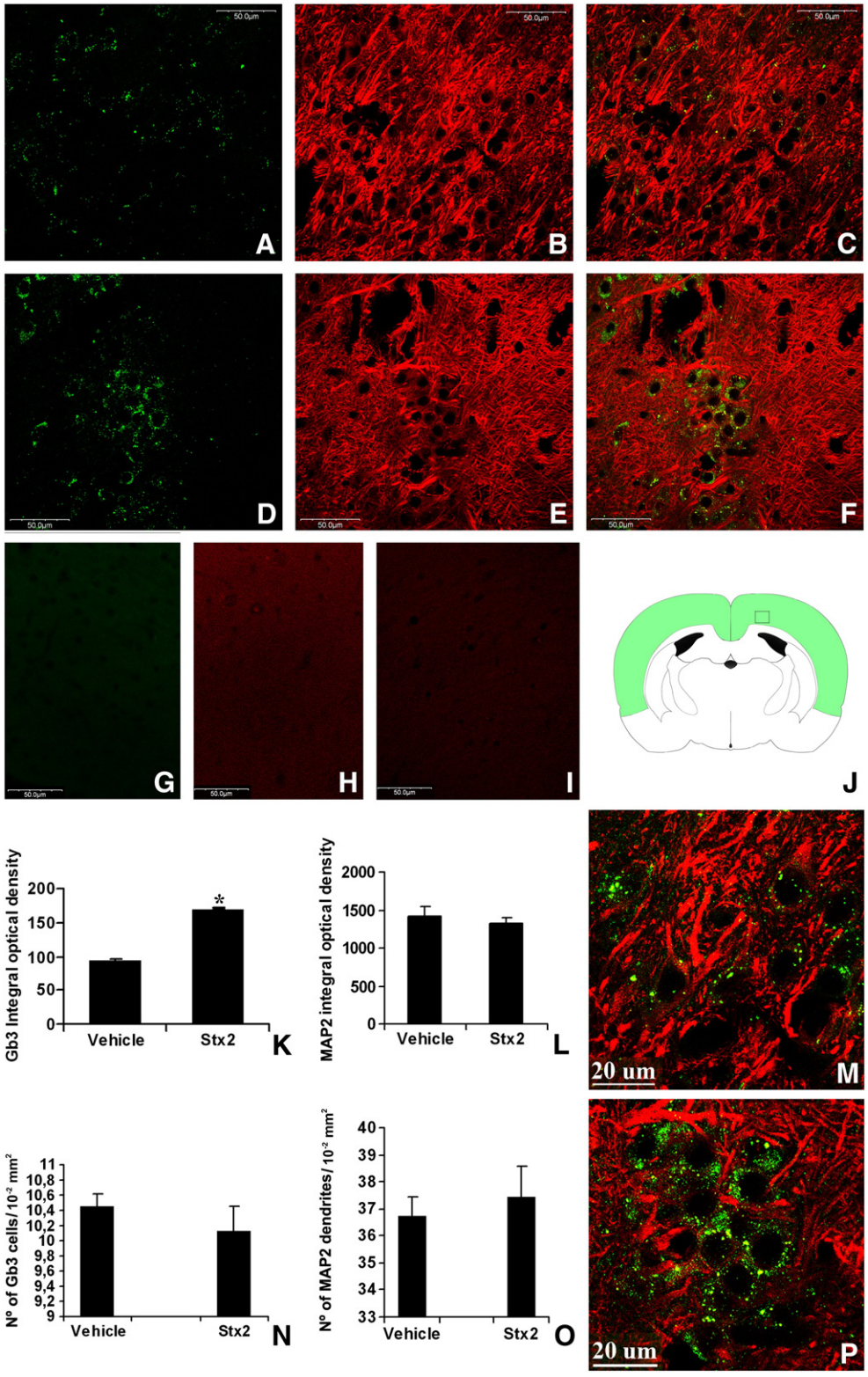

Fig. 8. The local administration of Stx2 increased the expression of the receptor Gb_3 in the rat inner cortex. Confocal immunofluorescence micrographs for Gb_3 and MAP2 are shown in green (A and D) and red (B and E) respectively, and merging images are observed in C and F. Representative vehicle- (A–C) and Stx2-treated (D–F) animals are shown. Stx2 increased the expression of Gb_3 (D) in neurons. Isotype controls micrographs for Gb_3 and MAP2 (G and H) showed no immunoreaction. A negative control for MAP2 is shown (I). The area observed in this study is marked in J. All these data were confirmed by IOD analysis, in which Stx2 induced the expression of Gb_3 (K), while no significant differences were found between both groups in the number of positive Gb_3 cells per field (N), MAP2 intensity (L) and also in the number of MAP2 immunopositive dendrites (O) after Stx2 i.c.v. administration. Cells were identified by using Hoechst nuclear staining (representative micrographs of nuclear fluorescent staining can be visualized in Fig. 11). A higher magnification of micrographs from vehicle- (M) or Stx2-treated (P) brains can be observed. The increased immunoexpression of Gb_3 is evidenced. Statistical significance is shown with an asterisk, $p<0.05$.

3.5. Increased neuronal expression of Gb_3 after i.c.v. Stx2 administration was immunolocalized in brain regions of reactive astrocytes

Confocal images showed that local administration of Stx2 induced the expression of Gb_3 in a circumscribed region of the striatum, in which reactive astrocytes were observed (Fig. 9D–F). No reactive astrocytes were observed in controls in a region almost devoid of Gb_3 (Fig. 9A–C). Then, in this region the induction of Gb_3 coincided with the immunolocalization of reactive astrocytes (Fig. 9F). Also, the expression of the Gb_3 receptor was immunolocalized in patches in astrocytic processes in the dorsal striatum (Fig. 9F) and it was absent in non-reactive astrocyte controls (Fig. 9C). One possibility for this Gb_3 topography is that some neuronal processes or bodies containing the receptor might be in contact with the reactive astrocytes, thus displaying the yellow merge color (Fig. 9F). Some Gb_3 receptors evidenced in green (Fig. 9D) were not immunolocalized in reactive astrocytes (Fig. 9E), probably due to their localization in neuronal fibers and bodies (Fig. 9D). Significant differences were obtained when reactive astrocytes in Stx2-treated striata were compared with those from the vehicle-treated ones and measured by IOD (Fig. 9J).

Gb_3 expression was also immunodetected in the microvasculature (Fig. 9G) at astrocytic endfeet processes (Fig. 9G–I). Astrocytic endfeet might be defined by immunofluorescence using an anti-GFAP antibody (red) (Fig. 9H) in contact with the microvasculature. At this point, Gb_3 expression was found in endothelial cells in apposition with astrocytic endfeet (Fig. 9I). Isotype and negative controls for

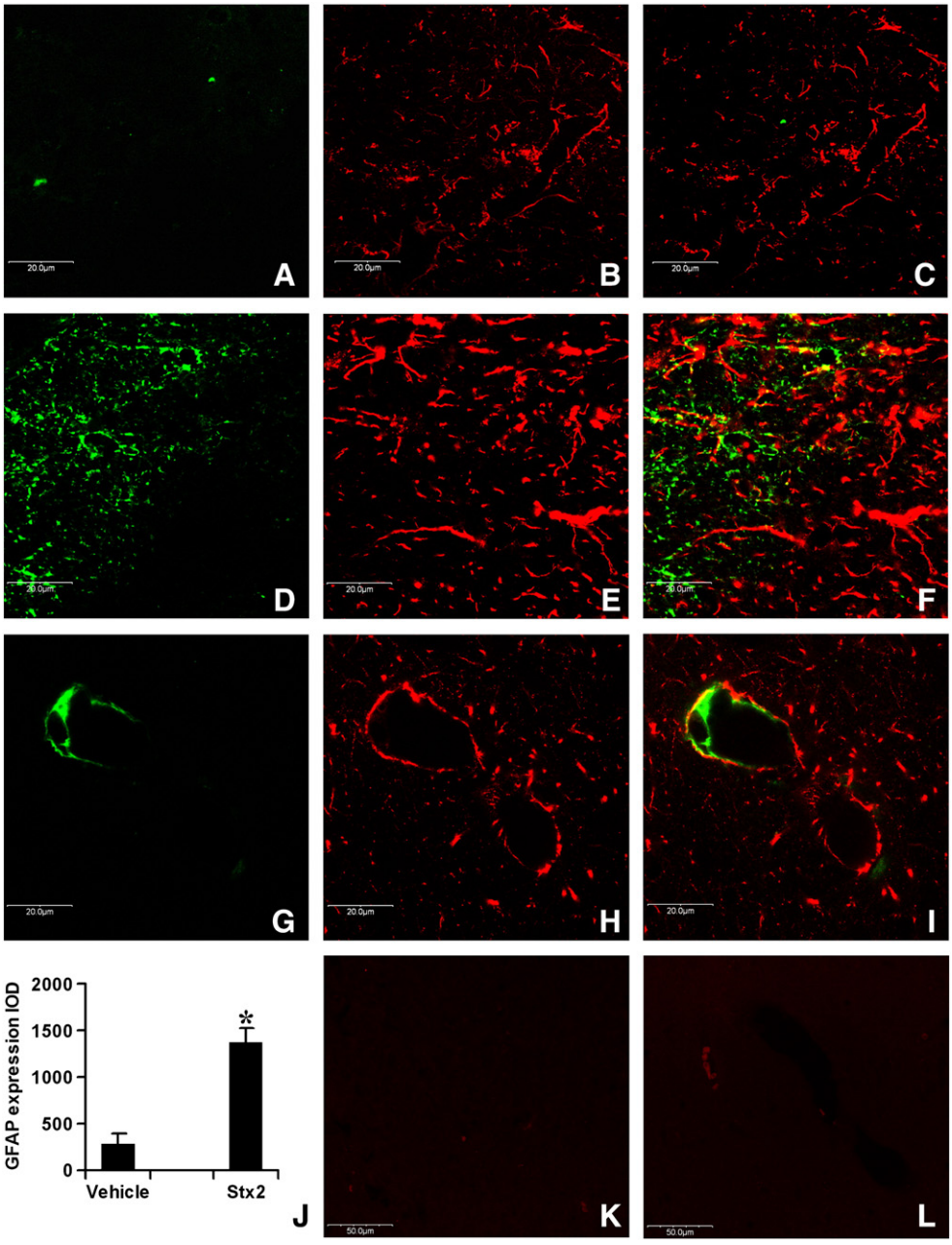

Fig. 9. Increased expression of Gb_3 in a reactive astrocytic area. Micrographs in higher magnification from vehicle- (A–C) and Stx2-treated (D–F) rat striata show confocal immunofluorescence for Gb_3 in green (A, D and G), and GFAP in red (B, E and H) and merge images for Gb_3 and GFAP immunoexpressions (C, F and I). Reactive astrocytes can be observed in the Stx2-treated brains (E) but not in the vehicle-treated ones (B). Gb_3 was immunolocalized in patches in astrocytic reactive processes (F) and was absent in non-reactive astrocyte controls (C). A higher-magnification micrograph showing the expression of Gb_3 (G) between an astrocytic end foot (H) and the endothelium can be observed (I). Densitometry of GFAP expression between vehicle and Stx2 treatments confirmed immunofluorescence images for reactive astrocytes (J). Isotype and negative controls for GFAP (K and L).

GFAP immunofluorescence showed no immunoreaction, thus validating the technique (Fig. 9K, L).

In the subfornical organ (Fig. 10I) reactive astrocytes were also found in Stx2-treated rats (Fig. 10E, K) in comparison with vehicle-treated ones (Fig. 10B, K) together with high expression of Gb_3 receptor (Fig. 10D, F, G, J). The Gb_3 receptor was also found in reactive astrocytic processes that contacted Gb_3 containing neurons (in yellow) (Fig. 10F) but not in controls (Fig. 10C). Isotype control in the subfornical area was performed and no immunofluorescence was obtained thus validating the technique used (Fig. 10H).

3.6. The receptor Gb_3 colocalized with Stx2 in neurons

We have previously demonstrated that Stx2 is able to pass the blood brain barrier (Goldstein et al., 2007), and have immunolocalized Stx2 in brain cells after its i.c.v administration (Boccoli et al., 2008). In the present paper, using immunofluorescence deconvolution microscopy we demonstrated that in rat brains Stx2 colocalized with its Gb_3 receptor in neurons after its i.c.v. administration. This was evident in dorsal striatal (Fig. 11E–H) and hippocampal CA1 layer (Fig. 11I–L) neurons. Vehicle-treated brains did not show this colocalization (Fig. 11A–D). Double localization performed by immunofluorescence deconvolution microscopy of Stx2 and its receptor Gb_3 was observed in subneuronal compartments in the striatum and hippocampus of toxin-treated animals (Fig. 11H, L). Some striatal neurons did not show Gb_3 immunofluorescence (Fig. 11H) probably due to technical limitations. The presented immunofluorescence deconvoluted microphotographs clearly supported that toxin-treated dorsal striatum expressed relatively more Gb_3 receptor than the vehicle-treated ones (Fig. 11E, A respectively).

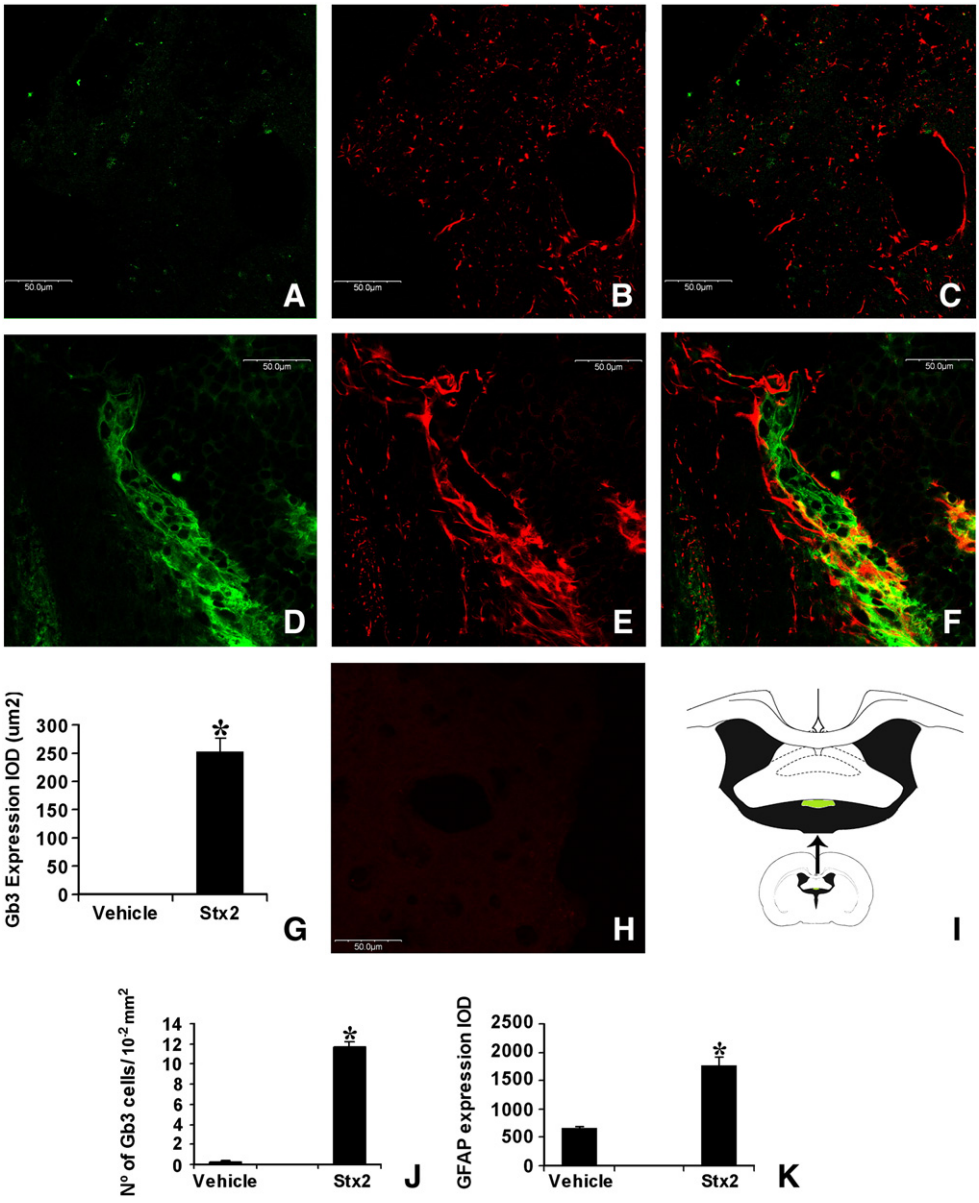

Fig. 10. Increased expression of neuronal Gb_3 and reactive astrocytes in the subfornical area. Micrographs in higher magnification from vehicle- (A–C) and Stx2-treated (D–F) rat subfornical organs show confocal immunofluorescence for Gb_3 in green (A and D), and GFAP in red (B and E) and merge images for Gb_3 and GFAP immunoexpressions (C and F). Reactive astrocytes can be observed in Stx2-treated brains (E) but not in the vehicle-treated ones (B). Gb_3 colocalized in some reactive astrocytic processes (yellow) in contact with Gb_3 positive neurons (green) (F) and was absent in non-reactive astrocyte controls (C). Significant densitometry for GFAP expression between vehicle and Stx2 treatments confirmed immunofluorescence images for reactive astrocytes (K). Isotype control for GFAP (H). Increased expression of Gb_3 in Stx2-treated subfornical areas was confirmed by IOD analysis (G), together with a higher number of positive Gb_3 cells per field (J). The area observed in this study is shown (I). Statistical significance is shown with an asterisk, $p<0.05$.

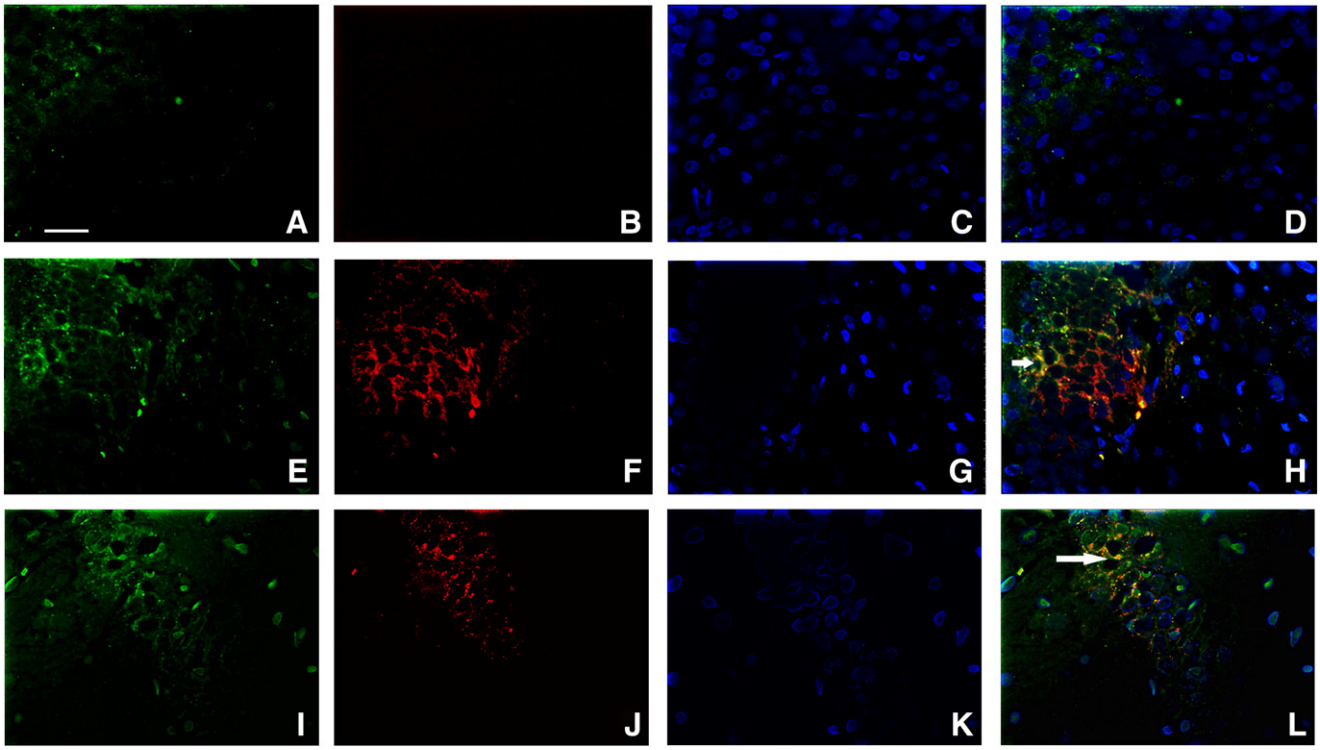

Fig. 11. Stx2 colocalized with Gb_3 in neurons after i.c.v. administration of the toxin. Deconvolution inmunofluorescence microscopy performed for Gb_3 (A, E and I), Stx2 (B, F and J), and Hoescht nuclear staining (C, G and K). Merging images are shown (D, H and L). Vehicle-treated striatal areas (A–D), Stx2 treatment of striatal areas (E–H) and hippocampal CA1 layer treated with Stx2 (I–L). Stx2 colocalized with its Gb_3 receptor in neurons (yellow) after the i.c.v. administration of the toxin as shown in H and L (arrows), while this was not observed in vehicle controls (D). Scale Bar = 30 um in A–L.

3.7. The pro-apoptotic protein Bax was immunolocalized in various cell brain regions after the i.c.v. administration of Stx2

The topographical distribution of the pro-apoptotic Bax protein found in neuronal and other cell populations of the cerebral cortex, hippocampal CA1 layer, subventricular zone, and third periventricular areas (Fig. 12) coincided with diffused regions of Stx2 after its i.c.v. administration. Bax immunoexpression was observed in neuronal populations of the inner cortex (Fig. 12B), and, in a higher magnification, immunolocalization of this protein was observed in cytoplasms and fibers (Fig. 12C). Bax was also expressed in the cytoplasm of hippocampal CA1 neurons (Fig. 12F, G). Immunoexpression of Bax in the subventricular regions (Fig. 12J) was only observed in the cytoplasm of cells limiting the lateral ventricle at the dorsal striatum (Fig. 12K). At the third ventricle level the expression of the pro-apoptotic protein was found in the cytoplasms of periventricular and ependymal cells (Fig. 12N). Bax pro-apoptotic neurons were not immunodetected in brains administered with the vehicle (Fig. 12A, E, I, M). Negative controls in the observed regions for Bax confocal immunofluorescence were performed and no immunosignal was obtained (Fig. 12D, H, L, O).

4. Discussion

In the present paper, we aimed to gain new insights into the understanding of the role of the Stx2 receptor Gb_3 on the etiology triggered by this toxin when it reaches the CNS, by studying the expression of neuronal Gb_3 after i.c.v. administration of Stx2 or a vehicle solution in rat brains. We found strong evidence supporting the hypothesis that the expression of Gb_3 in rat brains is upregulated after local toxin administration, and may thus be involved in brain damage by affecting neuronal and glial functional states.

The expression of Gb_3 was detected by confocal immunofluorescence in different brain areas. To our knowledge, this is the first evidence of Gb_3 neuronal localization in different rat brain neuronal populations.

In the present work the extent of LPS included in the Stx2 purification used to study the toxin effect on the expression of Gb_3 in the brain after i.c.v. injection did not change the expression levels of Gb_3 in CA1 neurons of the hippocampus. This was verified after the i.c.v. injection of the same Stx2 lot in which LPS was removed. The rats were kept in the same initial conditions. Moreover, the commercial LPS used did not enhance Gb_3 expression as compared to controls, in the amount that originally contained the Stx2 solution. Although it has been reported that different combinations of LPS with Shiga toxin result in a synergistic cytotoxic effect in human vascular endothelial cells *in vitro* (Louise and Obrig, 1992), this is not the case for our i.c.v. model. Synergism in that study was observed at LPS concentrations between 0.1 and 1.0 μg/ml and LPS alone was cytotoxic at 10 μg/ml (Stone et al., 2008), while the LPS extent in our current work was 0.05 μg/ml. Conversely, synergistic cytotoxicity was not observed by Tesh et al. (1991) in human endothelial veins. In light of our results, this synergistic action found *in vitro* with other cell types other than neurons was not observed in our work. The synergistic effects observed in *in vitro* experiments may usually not reflect the *in vivo* conditions. However, it cannot be discarded that LPS may be involved in Gb_3 neuronal expression, but not under our experimental conditions.

The i.c.v. technique used in this paper allowed us to microinfuse the toxin in a specific brain area of interest by using a stereotaxic frame. We placed the cannula in the lateral ventricle to avoid mechanical tissue damage. The techniques used to observe Stx2-immunopositive neurons were validated from a previous paper by us, in which the capacity of Stx2 to invade the brain was tested. Stx2 immunolocalization was observed in neurons, but not with the incubation of an isotype antibody

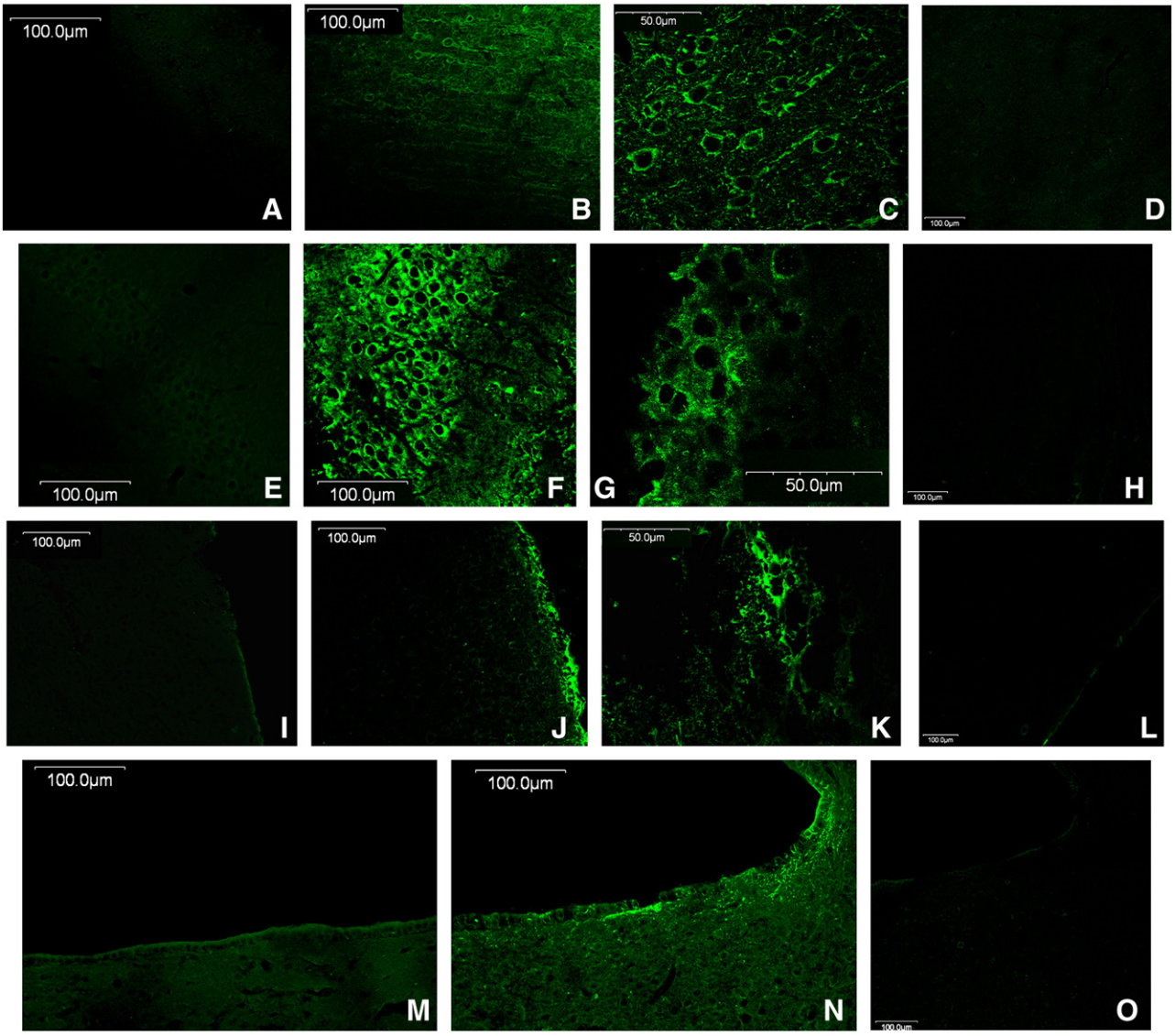

Fig. 12. Stx2 induced the expression of the pro-apoptotic protein Bax 2 in neurons after its i.c.v. administration. Bax was not immunodetected in vehicle-treated brains (A, E, I and M). Bax immunoexpression was detected in the inner cortex (B), and immunolocalization of this protein was observed in neuronal cytoplasms and fibers shown in a higher-magnification micrograph (C). In addition immmunoexpression of this protein was observed in neurons and other cell types of CA1 hippocampus (F), subventricular region of the dorsal striatum (J), and the hypothalamic periventricular area (N). Higher-magnification micrographs of the hippocampus and dorsal striatum are shown (G and K). Negative controls in the studied regions presented no immunofluorescence (D, H, L and O).

used as a control for Stx2 immunohistochemistry, nor by omitting a primary antibody (Goldstein et al., 2007). These techniques were corroborated by the different controls performed in that paper. Moreover, in a subsequent work where reactive astrocytes were identified in a damaged neuronal area of the hippocampus following i.c.v. administration of Stx2, additional Stx2 immunopositive neuron controls were performed for the same immunofluorescence technique used to identify Stx2 immunopositive neurons. A negative immunofluorescence signal was obtained when vehicle was used as control, a concentration-dependent post-Stx2 binding signal was obtained in fixed brain tissue, and pre-incubating the toxin with a saturated concentration of an anti-Stx2B antibody prevented the toxin from binding neurons (Boccoli et al., 2008). The concentration of toxin used in this work was 24 pg/g of body weight by i.c.v. injection and was in the range of similar amounts used by other authors of different STEC animal models of disease. The amounts of Stx2 were between 250 pg/g (Mizuguchi et al., 1996) and 5000 pg/g of body weight (Fujii et al., 1996, 1998) by intravenous injection and starting from 0.4 pg/g of body weight (Mizuguchi et al., 1996) by intrathecal injection which resulted in a strong toxic effect and caused brain damage. Mizuguchi et al. (1996) reported that Stx2 concentration in cerebro-spinal fluid (CSF) increases during the initial 6 h in rabbits after an intravenous Stx2 injection at the dose of 6 μg/head, peaking at 200–300 pg/ml. Also, Fujii et al. (1998) determined a Stx2 concentration between 100 and 1000 pg/ml in CSF in the initial hours after an intravenous injection of 5 μg/kg of the toxin.

In the cortex, striatum and hippocampus Gb_3 expression increased after Stx2 administration in neurons. This was accompanied by an increase in the expression of MAP2, a cytoskeletal protein found in neuronal cytoplasm and dendrites in immunopositive Gb_3 neurons. Under physiological conditions, MAP2 may be involved in the modulation of synaptic plasticity (Sánchez et al., 2000). In pathological conditions over-expression of MAP2 and growth of dendrites can be found due to excessive neurotransmitter release in response to seizure activity in specific areas of the adult brain (Kato et al., 2001). Excessive neurotransmitter release is also produced in neurons after treatment with Stx2 in murine brain slices (Obata et al., 2008).

Two pathological features in dendrites were observed in the present paper: dendritic thickening (Figs. 5 and 6) and focal dendritic

swelling (Fig. 7) in injured neurons. The first was previously described using immunoreactivity against MAP2 in CA1 hippocampal brains from schizophrenic patients (Cotter et al., 2000), following seizure activity (Pei et al., 1998), or after electrical stimulation (Zhou et al., 2010) in animal models. The latter was observed in neurons after NMDA exposure in which a change in the distribution of MAP2 was evidenced. Focal swelling decreased in distal dendrites and increased in neuronal somata and proximal dendrites (Faddis et al., 1997). A consequence of focal swelling is dendritic spine loss, and lack of synaptic axonal connections. This is related to the abnormal organization of cytoskeletal dendritic proteins that may occur in brain edema situations (Fiala et al., 2002), which coincides with other described cases of brain edema in patients intoxicated with STEC (Barnett et al., 1995) and in animal models of Stx2 intoxication (Fujii et al., 1994; Francis et al., 1989). Therefore, dendritic thickening and focal swelling can be readily measured by confocal immunofluorescence using a MAP2 antibody with a software image analyzer. The pathological dendritic changes that occurred following i.c.v. administration of Stx2 may be due, among other causes, to cytoskeletal remodeling including MAP2. This event has also been observed following cerebral ischemia (Zhou et al., 2010; Bidmon et al., 1998). These data coincide with a previous ultrastructural finding of hypertrophied dendrites containing augmented protein densities following i.c.v. administration of Stx2, (Goldstein et al., 2007).

After Stx2 treatment, Gb_3 immunolocalization was also observed in reactive astrocytic processes surrounding neurons in the rat brain immunostained with GFAP, between astrocytes end feet and endothelial cells and in cells of subfornical organ. In a previous report we found that Stx2 changed the expression levels of striatal astrocytic GFAP in a dose–response effect (Boccoli et al., 2008). Confocal colocalization between GFAP protein and Gb3 may be attributable to neuronal processes containing Gb_3 in physical touch with astrocytes. Another possibility is the presence of a glial Gb_3 receptor. However, the presence of this receptor in this kind of cells has not yet been established. Interestingly, immunolocalization of the receptor is not found in non-reactive astrocytes from vehicle-treated rat brains. While some authors claim that reactive astrocytes may exert a neuroprotective role (Sakuma et al., 2008), others supported that reactive astrocytes may produce neuronal loss (Lei et al., 1996; Liu et al., 2006; Dupuis et al., 2008).

In the present work we also demonstrated that neurons expressing Gb_3 colocalize with endocytosed Stx2 in the striatum and the hippocampus. The technique used to observe Stx2-immunopositive neurons was validated from a previous paper by us (Goldstein et al., 2007). The involvement of cytokines in Gb_3 induction and consequently in cell death by Stx has already been determined in other cell types (Eisenhauer et al., 2001; Stricklett et al., 2002). It has been shown that astrocytes may release mediators like cytokines (Ridet et al., 1997) or neurotrophic factors (Pehar et al., 2004; Cassina et al., 2005) that could be neurotoxic to neurons pursuing brain damage. Active participation of cytokines or neurotrophic factors in the current i.c.v. Stx2 model is highly probable, and remains an open question that we are currently assessing.

Neurons leading to apoptosis are demonstrated by the expression of the pro-apoptotic Bax protein. Activation of pro-apoptotic proteins such as Bax may indicate or cause mitochondrial damage after brain ischemia (Liu et al., 2004). The pro-apoptotic cell condition determined by Bax has been investigated by other authors after Stx administration (Jones et al., 2000; Johansson et al., 2006). In the present paper the regional distribution of Bax immunoexpression in neurons and other cell populations includes the cortex, the hippocampus, and subventricular and periventricular regions, including ependymal cells from the hypothalamic third ventricle. These regions are circumscribed topographically next to the ventricles. Current immunoexpression of Bax in neurons may support a previously characterized apoptotic condition caused by the toxin (Goldstein et al., 2007). Herein we describe neurons expressing Bax in the striatum and motor-associated cortex, the main brain regions associated with motor movement (Bolam et al., 2000), which coincide with the expression of Gb_3 in neurons in the same brain regions after toxin treatment. The striatum is mainly involved in HUS patients that suffered from hemiparesis, seizures, coma, altered mental state or tremor (Steinborn et al., 2004; Barnett et al., 1995). Damage to striatum neurons observed in our model could contribute to hypokinesia, a manifestation of motor dysfunction found in experimental parkinsonism models (Bolam et al., 2000). Therefore, Stx2 may affect motor movement from neurons that control superior brain levels.

The toxin-treated animals tended to gain weight as compared to their initial weight, which may reflect an absence of renal involvement of this model. In other studies, in which Stx2 is administered via systemic route, animals lose weight as compared to their initial weight, and according to Psotka et al. (2009) this is due to renal dysfunction. However, Stx2-treated rats developed CNS symptoms and died.

The observed animal weight loss after toxin i.c.v. administration compared to controls may underlie autonomic and/or endocrine dysfunctions for energy balance in medial hypothalamus (Lechan and Fekete, 2006). For instance nitric oxide from the hypothalamic paraventricular nucleus may regulate the expression of neuropeptides involved in energy balance and in cachexia under pathological conditions (Wang et al., 2005). The presence of Stx2 in the brain increased the expression of nitric oxide in neurons from this region (Boccoli et al., 2008) and could be related to weight variation. Another reason for this weight variation could be the action of cytokines in melanocortin signaling in the hypothalamus under inflammatory or chronic diseased conditions (Scarlett et al., 2007), a state that the toxin treatment may trigger.

The mechanistic action of this toxin, in which neuronal and glial cells derive to a degenerative condition, the role performed by the Gb_3 receptor that underlies this cell condition and the local cytokines potentially involved that may be produced in the event are a current matter of study.

In summary, the i.c.v. administration of Stx2 increases the expression of neuronal Gb_3 in different rat brain areas. This action may produce altered functional states in neurons observed at postsynapsis, since an increased dendritic size immunostained with MAP2 was evident. Reactive astrocytes may exert either a protective or a neurotoxic role in brain damage, although Bax expression may support a neurotoxic event. The results obtained with Stx2 in this animal model may explain the encephalopathies observed in some patients affected by HUS, being the Gb_3 receptor one of the most important potential candidates to mediate Stx2 neurotoxicity.

Acknowledgments

These studies were supported by the CONICET Argentina (National Research Council) grants PIP5588 and PIP114-200801-00497 and the Universidad de Buenos Aires grant UBACyT/M420 to J. Goldstein.

References

Barnett, N.D.P., Kaplan, A.M., Bernes, S.M., Cohen, M.L., 1995. Hemolytic uremic syndrome with particular involvement of basal ganglia and favorable outcome. Pediatr. Neurol. 12, 155–158.

Bidmon, H.J., Jancsik, V., Schleicher, A., Hagemann, G., Witte, O.W., Woodhams, P., Zilles, K., 1998. Structural alterations and changes in cytoskeletal proteins and proteoglycans after focal cortical ischemia. Neuroscience 82, 397–420.

Boccoli, J., Loidl, C.F., Lopez-Costa, J.J., Creydt, V.P., Ibarra, C., Goldstein, J., 2008. Intracerebroventricular administration of Shiga toxin type 2 altered the expression levels of neuronal nitric oxide synthase and glial fibrillary acidic protein in rat brains. Brain Res. 1230, 320–333.

Bolam, J.P., Hanley, J.J., Booth, P.A., Bevan, M.D., 2000. Synaptic organisation of the basal ganglia. J. Anat. 196, 527–542.

Candiano, G., Bruschi, M., Musante, L., Santucci, L., Ghiggeri, G.M., Carnemolla, B., Orecchia, P., Zardi, L., Righetti, P.G., 2004. Blue silver: a very sensitive colloidal Coomassie G-250 staining for proteome analysis. Electrophoresis 25, 1327–1333.

Cassina, P., Pehar, M., Vargas, M.R., Castellanos, R., Barbeito, A.G., Estevez, A.G., Thompson, J.A., Beckman, J.S., Barbeito, L., 2005. Astrocyte activation by fibroblast growth factor-1 and motor neuron apoptosis: implications for amyotrophic lateral sclerosis. J. Neurochem. 93, 38–46.

Cotter, D., Wilson, S., Roberts, E., Kerwin, R., Everall, I.P., 2000. Increased dendritic MAP2 expression in the hippocampus in schizophrenia. Schizophr. Res. 41, 313–323.

Dupuis, L., Pehar, M., Cassina, P., Rene, F., Castellanos, R., Rouaux, C., Gandelman, M., Dimos, L., Schwab, M.E., Loeffler, J.P., Barbeito, L., Gonzalez de Aguilar, J.L., 2008. Nogo receptor antagonizes p75NTR-dependent motor neuron death. Proc. Natl Acad. Sci. USA 105, 740–745.

Eisenhauer, P.B., Chaturvedi, P., Fine, R.E., Ritchie, A.J., Pober, J.S., Cleary, T.G., Newburg, D.S., 2001. Tumor necrosis factor alpha increases human cerebral endothelial cell Gb_3 and sensitivity to Shiga toxin. Infect. Immun. 69, 1889–1894.

Eriksson, K.J., Boyd, S.G., Tasker, R.C., 2001. Acute neurology and neurophysiology of haemolytic–uraemic syndrome. Arch. Dis. Child. 84, 434–435.

Faddis, B.T., Hasbani, M.J., Goldberg, M.P., 1997. Calpain activation contributes to dendritic remodeling after brief excitotoxic injury in vitro. J. Neurosci. 17, 951–959.

Falguieres, T., Johannes, L., 2006. Shiga toxin B-subunit binds to the chaperone BiP and the nucleolar protein B23. Biol. Cell 98, 125–134.

Falguières, T., Mallard, F., Baron, C., Hanau, D., Lingwood, C., Goud, B., Salamero, J., Johannes, L., 2001. Targeting of Shiga toxin B-subunit to retrograde transport route in association with detergent-resistant membranes. Mol. Biol. Cell 12, 2453–2468.

Fiala, J.C., Spacek, J., Harris, K.M., 2002. Dendritic spine pathology: cause or consequence of neurological disorders? Brain Res. Brain Res. Rev. 39, 29–54.

Francis, D.H., Moxley, R.A., Andraos, C.Y., 1989. Edema disease-like brain lesions in gnotobiotic piglets infected with *Escherichia coli* serotype O157:H7. Infect. Immun. 57, 1339–1342.

Fujii, J., Kita, T., Yoshida, S., Takeda, T., Kobayashi, H., Tanaka, N., Ohsato, K., Mizuguchi, Y., 1994. Direct evidence of neuron impairment by oral infection with verotoxin-producing *Escherichia coli* O157:H- in mitomycin-treated mice. Infect. Immun. 62, 3447–3453.

Fujii, J., Kinoshita, Y., Kita, T., Higure, A., Takeda, T., Tanaka, N., Yoshida, S., 1996. Magnetic resonance imaging and histopathological study of brain lesions in rabbits given intravenous verotoxin 2. Infect. Immun. 64, 5053–5060.

Fujii, J., Kinoshita, Y., Yamada, Y., Yutsudo, T., Kita, T., Takeda, T., Yoshida, S., 1998. Neurotoxicity of intrathecal Shiga toxin 2 and protection by intrathecal injection of anti-Shiga toxin 2 antiserum in rabbits. Microb. Pathog. 25, 139–146.

Fujii, J., Matsui, T., Heatherly, D.P., Schlegel, K.H., Lobo, P.I., Yutsudo, T., Ciraolo, G.M., Morris, R.E., Obrig, T., 2003. Rapid apoptosis induced by Shiga toxin in HeLa cells. Infect. Immun. 71, 2724–2735.

Fujii, J., Wood, K., Matsuda, F., Carneiro-Filho, B.A., Schlegel, K.H., Yutsudo, T., Binnington-Boyd, B., Lingwood, C.A., Obata, F., Kim, K.S., Yoshida, S., Obrig, T., 2008. Shiga toxin 2 causes apoptosis in human brain microvascular endothelial cells via C/EBP homologous protein. Infect. Immun. 76, 3679–3689.

Goldstein, J., Loidl, C.F., Creydt, V.P., Boccoli, J., Ibarra, C., 2007. Intracerebroventricular administration of Shiga toxin type 2 induces striatal neuronal death and glial alterations: an ultrastructural study. Brain Res. 1161, 106–115.

Johannes, L., Decaudin, D., 2005. Protein toxins: intracellular trafficking for targeted therapy. Gene Ther. 16, 1360–1368.

Johansson, D., Johansson, A., Grankvist, K., Andersson, U., Henriksson, R., Bergström, P., Brännström, T., Behnam-Motlagh, P., 2006. Verotoxin-1 induction of apoptosis in Gb3-expressing human glioma cell lines. Cancer Biol. Ther. 5, 1211–1217.

Jones, N.L., Islur, A., Haq, R., Mascarenhas, M., Karmali, M.A., Perdue, M.H., Zanke, B.W., Sherman, P.M., 2000. *Escherichia coli* Shiga toxins induce apoptosis in epithelial cells that is regulated by the Bcl-2 family. Am. J. Physiol. Gastrointest. Liver Physiol. 278, G811–G819.

Karmali, M.A., 2004. Infection by Shiga toxin-producing *Escherichia coli*: an overview. Mol. Biotechnol. 26, 117–122.

Kato, K., Masa, T., Tawara, Y., Kobayashi, K., Oka, T., Okabe, A., Shiosaka, S., 2001. Dendritic aberrations in the hippocampal granular layer and the amygdalohippocampal area following kindled-seizures. Brain Res. 901, 281–295.

Lechan, R.M., Fekete, C., 2006. The TRH neuron: a hypothalamic integrator of energy metabolism. Prog. Brain Res. 153, 209–235.

Lei, D.L., Yang, D.L., Liu, H.M., 1996. Local injection of kainic acid causes widespread degeneration of NADPH-d neurons and induction of NADPH-d in neurons, endothelial cells and reactive astrocytes. Brain Res. 19, 199–206.

Liu, C.L., Siesjo, B.K., Hu, B.R., 2004. Pathogenesis of hippocampal neuronal death after hypoxia-ischemia changes during brain development. Neuroscience 127, 113–123.

Liu, X., Sullivan, K.A., Madl, J.E., Legare, M., Tjalkens, R.B., 2006. Manganese-induced neurotoxicity: the role of astroglial-derived nitric oxide in striatal interneuron degeneration. Toxicol. Sci. 91, 521–531.

Lord, J.M., Roberts, L.M., Lencer, W.I., 2005. Entry of protein toxins into mammalian cells by crossing the endoplasmic reticulum membrane: co-opting basic mechanisms of endoplasmic reticulum-associated degradation. Curr. Top. Microbiol. Immunol. 300, 149–168.

Louise, C.B., Obrig, T.G., 1991. Shiga toxin-associated hemolytic-uremic syndrome: combined cytotoxic effects of Shiga toxin, interleukin-1 beta, and tumor necrosis factor alpha on human vascular endothelial cells in vitro. Infect. Immun. 59, 4173–4179.

Louise, C.B., Obrig, T.G., 1992. Shiga toxin-associated hemolytic uremic syndrome: combined cytotoxic effects of shiga toxin and lipopolysaccharide (endotoxin) on human vascular endothelial cells in vitro. Infect. Immun. 60, 1536–1543.

Mallard, F., Antony, C., Tenza, D., Salamero, J., Goud, B., Johannes, L., 1998. Direct pathway from early/recycling endosomes to the Golgi apparatus revealed through the study of shiga toxin B-fragment transport. J. Cell Biol. 143, 973–990.

Mizuguchi, M., Tanaka, S., Fujii, I., Tanizawa, H., Suzuki, Y., Igarashi, T., Yamanaka, T., Takeda, T., Miwa, M., 1996. Neuronal and vascular pathology produced by verocytotoxin 2 in the rabbit central nervous system. Acta Neuropathol. 91, 254–262.

Obata, F., Tohyama, K., Bonev, A.D., Kolling, G.L., Keepers, T.R., Gross, L.K., Nelson, M.T., Sato, S., Obrig, T.G., 2008. Shiga toxin 2 affects the central nervous system through receptor globotriaosylceramide localized to neurons. J. Infect. Dis. 198, 1398–1406.

O'Brien, A.D., Kaper, J.B., 1998. Shiga toxin-producing *Escherichia coli*: yesterday, today, and tomorrow. In: Kaper, J.B., O'Brien, A.D. (Eds.), *Escherichia coli* O157:H7 and Other Shiga Toxin-Producing *E. coli* Strains. Am. Soc. Microbiology. Washington, DC, pp. 1–11.

Tesh, V.L., Samuel, J.E., Perera, L.P., Sharefkin, J.B., O'Brien, A.D., 1991. Evaluation of the role of Shiga and Shiga-like toxins in mediating direct damage to human vascular endothelial cells. J Infect. Dis. 164, 344–352.

Okuda, T., Nakayama, K., 2008. Identification and characterization of the human Gb3/CD77 synthase gene promoter. Glycobiology 18, 1028–1035.

Paton, J.C., Paton, A.W., 1998. Pathogenesis and diagnosis of Shiga toxin-producing *Escherichia coli* infections. Clin. Microbiol. Rev. 11, 450–479.

Paxinos, G., Watson, C., 2005. The Rat Brain in Stereotaxic CoordinatesFifth Edition. Elsevier Academic Press, Burlington, MA, U.S.A.

Pehar, M., Cassina, P., Vargas, M.R., Castellanos, R., Viera, L., Beckman, J.S., Estevez, A.G., Barbeito, L., 2004. Astrocytic production of nerve growth factor in motor neuron apoptosis: implications for amyotrophic lateral sclerosis. J. Neurochem. 89, 464–473.

Pei, Q., Burnet, P.J., Zetterström, T.S., 1998. Changes in mRNA abundance of microtubule-associated proteins in the rat brain following electroconvulsive shock. NeuroReport 9, 391–394.

Proulx, F., Seidman, E.G., Karpman, D., 2001. Pathogenesis of Shiga toxin-associated hemolytic uremic syndrome. Pediatr. Res. 50, 63–171.

Psotka, M.A., Obata, F., Kolling, G.L., Gross, L.K., Saleem, M.A., Satchell, S.C., Mathieson, P.W., Obrig, T.G., 2009. Shiga toxin 2 targets the murine renal collecting duct epithelium. Infect. Immun. 77, 959–969.

Ren, J., Utsunomiya, I., Taguchi, K., Ariga, T., Tai, T., Ihara, Y., Miyatake, T., 1999. Localization of verotoxin receptors in nervous system. Brain Res. 825, 183–188.

Ridet, J.L., Malhotra, S.K., Privat, A., Gage, F.H., 1997. Reactive astrocytes: cellular and molecular clues to biological function. Trends Neurosci. 20, 570–577.

Sakuma, M., Hyakawa, N., Kato, H., Araki, T., 2008. Time dependent changes of striatal interneurons after focal cerebral ischemia in rats. J. Neural Transm. 115, 413–422.

Sánchez, C., Díaz-Nido, J., Avila, J., 2000. Phosphorylation of microtubule-associated protein 2 (MAP2) and its relevance for the regulation of the neuronal cytoskeleton function. Prog. Neurobiol. 61, 133–168.

Sandvig, K., van Deurs, B., 2005. Delivery into cells: lessons learned from plant and bacterial toxins. Gene Ther. 12, 865–872.

Scarlett, J.M., Jobst, E.E., Enriori, P.J., Bowe, D.D., Batra, A.K., Grant, W.F., Cowley, M.A., Marks, D.L., 2007. Regulation of central melanocortin signaling by interleukin-1 beta. Endocrinology 148, 4217–4225.

Steinborn, M., Leiz, S., Rüdisser, K., Griebel, M., Harder, T., Hahn, H., 2004. CT and MRI in haemolytic uraemic syndrome with central nervous system involvement: distribution of lesions and prognostic value of imaging findings. Pediatr. Radiol. 34, 805–810.

Stone, M.K., Kolling, G.L., Lindner, M.H., Obrig, T.G., 2008. p38 mitogen-activated protein kinase mediates lipopolysaccharide and tumor necrosis factor alpha induction of shiga toxin 2 sensitivity in human umbilical vein endothelial cells. Infect. Immun. 76, 1115–1121.

Stricklett, P.K., Hughes, A.K., Ergonul, Z., Kohan, D.E., 2002. Molecular basis for up-regulation by inflammatory cytokines of Shiga toxin 1 cytotoxicity and globotriaosylceramide expression. J. Infect. Dis. 186, 976–982.

Takahashi, K., Funata, N., Ikuta, F., Sato, S., 2008. Neuronal apoptosis and inflammatory responses in the central nervous system of a rabbit treated with Shiga toxin-2. J. Neuroinflammation 5, 11. doi:10.1186/1742-2094-5-11.

Takenouchi, H., Kiyokawa, N., Taguchi, T., Matsui, J., Katagiri, Y.U., Okita, H., Okuda, K., Fujimoto, J., 2004. Shiga toxin binding to globotriaosyl ceramide induces intracellular signals that mediate cytoskeleton remodeling in human renal carcinoma-derived cells. J. Cell Sci. 117, 3911–3922.

Valles, P.G., Pesle, S., Piovano, L., Davila, E., Peralta, M., Principi, I., Lo, Giudice P., 2005. Postdiarrheal Shiga toxin-mediated hemolytic uremic syndrome similar to septic shock. Medicina 65, 395–401.

Wang, W., Svanberg, E., Delbro, D., Lundholm, K., 2005. NOS isoenzyme content in brain nuclei as related to food intake in experimental cancer cachexia. Brain Res. Mol. Brain Res. 134, 205–214.

Zhou, Q., Zhang, Q., Zhao, X., Duan, Y.Y., Lu, Y., Li, C., Li, T., 2010. Cortical electrical stimulation alone enhances functional recovery and dendritic structures after focal cerebral ischemia in rats. Brain Res. 1311, 148–157.